

Inflamed Leidenfrost drops

Xujun Fan^{*}


*College of Digital Technology and Engineering, [Ningbo University of Finance and Economics](#),
Ningbo 315175, China
and State Key Laboratory of Fluid Power and Mechatronic Systems, [Zhejiang University](#),
Hangzhou 310027, China*

Stéphane Dorbolo^{*}

FNRS-CESAM-PtYX laboratory, Département de Physique, [Université de Liège](#), Liège B-4000, Belgique

Fangye Lin[†]

Ningbo Innovation Center, [Zhejiang University](#), Ningbo 315100, China

Jun Zou^{‡}

*State Key Laboratory of Fluid Power and Mechatronic Systems, [Zhejiang University](#),
Hangzhou 310027, China*



(Received 18 December 2023; revised 20 August 2024; accepted 7 March 2025;
published 8 April 2025)

A Leidenfrost drop made of inflammable liquid exhibits increased evaporation when inflamed. Contrary to the classical Leidenfrost framework, the evaporation from the top part cannot be neglected anymore. Herein, we report the evaporation dynamics of an inflamed drop for various wall temperatures. The combustion duration is found to be significantly longer in the Leidenfrost state than below the Leidenfrost transition. For large drops, we show that we can split the evaporation of inflamed Leidenfrost drops into two independent systems: the bottom and top parts. Assuming that the bottom contribution does not depend on the combustion, the top contribution can be extracted and analyzed, which is observed (i) to remain smaller than the bottom contribution and (ii) to be constant in the temperature range considered. This implies that the top evaporation rate is solely due to the intrinsic burning rate of the flammable liquid at saturation temperature.

DOI: [10.1103/PhysRevFluids.10.043601](https://doi.org/10.1103/PhysRevFluids.10.043601)

I. INTRODUCTION

Evaporation and boiling of liquids [1] are common in various industrial applications and technologies, such as nuclear reactor cooling [2], inkjet printing [3], water mist fire suppression [4], and the manufacturing of semiconductor and microfluidic devices [5,6]. When a drop is released onto a horizontal wall, the heat transfer between the drop and the wall changes as the wall temperature T_w increases [7–9]. When T_w surpasses the liquid's boiling point T_b , there exists a transition known as Leidenfrost temperature T_{Leid} , for which a vapor film does stabilize between the drop and the wall, completely isolating the drop from the wall. This leads to a dramatic decrease in heat transfer while the drop floats over the wall surface, and it exhibits the well-known Leidenfrost

^{*}These authors contributed equally to this work.

[†]Contact author: linfy@zju.edu.cn

[‡]Contact author: junzou@zju.edu.cn

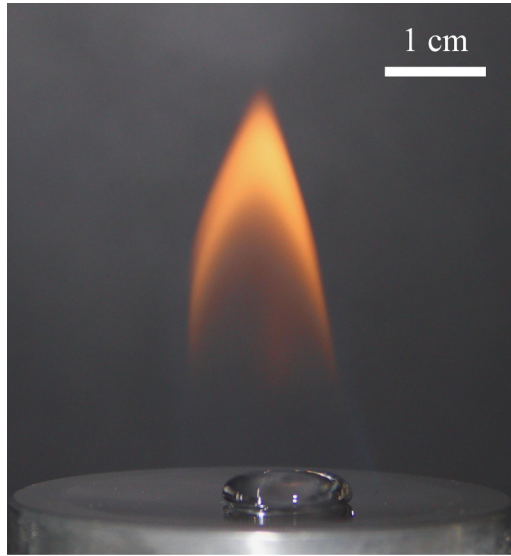


FIG. 1. Example of an inflamed Leidenfrost drop.

phenomenon [10]. This effect is sometimes reported as being problematic because of the heat transfer deterioration (e.g., nuclear cooling, fire, metallurgy quenching) but more rarely as an advantage because of the perfect nonwetting and high mobility of the drop (including drug delivery, thermal management, drag reduction, and laboratory-on-a-chip technology) [11–14], which arises from the unique properties of the Leidenfrost state conferred by the stable vapor film.

The generation and stability of this film depend on the thermal properties of the wall acting as the source of heat (in the case of the inverse Leidenfrost effect, the drop itself serves as the heat source [15]). The thermal properties of the walls and the roughness of its surface are crucial for the onset of the Leidenfrost state [16,17] and also for the thermalization of the cold impacting droplet [18]. The surface roughness is particularly unfavorable to the establishment of a stable vapor film, and consequently the Leidenfrost temperature increases with the roughness [19,20]. This stands in contrast to superhydrophobic surfaces, where the combination of roughness and hydrophobic coating can suppress the Leidenfrost transition [21]. On such surfaces, the heat transfer between the drop and the wall remains low, even at low temperatures, due to the presence of air between the drop and the wall since the drop is hanged to the tip of the roughness. On the other side of the roughness spectrum, when a solid wall is replaced by a liquid (smooth surface), the Leidenfrost temperature becomes comparable to the boiling point of the liquid [22], despite the less optimal thermal properties of liquids compared to solids [23]. In all the cited works, the evaporation from the upper part of the drop is neglected compared to the rapid evaporation occurring at the bottom through the vapor film.

In the context of flammable liquids, the mobility of the Leidenfrost drops is very unfavorable regarding the ignition and flame propagation, as highlighted by recent studies [24,25]. Therefore, the Leidenfrost effect proves to be crucial in scenarios involving energy and fire hazards [26–28], e.g., during the interaction of a burning drop with a hot wall in fuel spray combustion within an engine [29], or in the spread and evaporation of continuously impacting drops on a wall surface during a dripping fire [30]. A pertinent illustration of this is the behavior of a burning ethanol Leidenfrost drop, depicted in Fig. 1, which shows a hemispherical drop levitating above a heated aluminum plate. This scenario not only emphasizes the accelerated evaporation due to combustion but also raises critical questions regarding the potential for fire propagation facilitated by enhanced mobility of Leidenfrost drops.

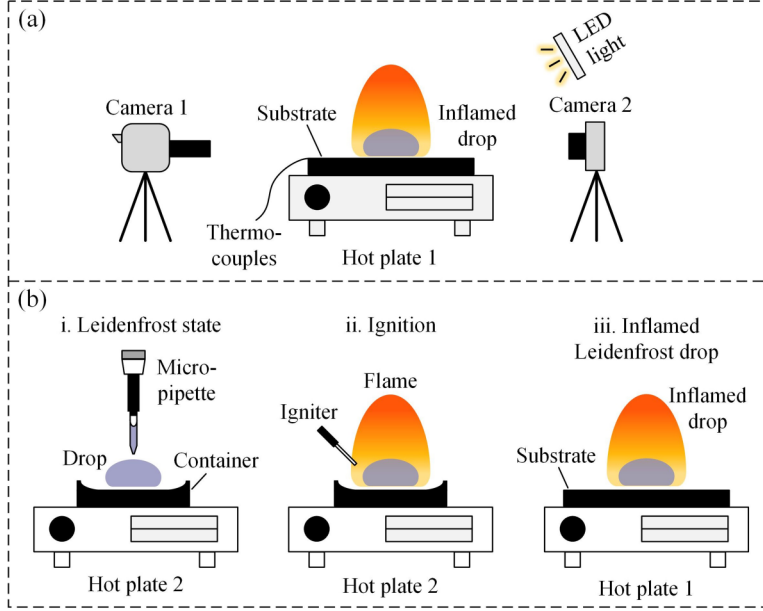


FIG. 2. (a) Experimental setup. (b) Procedure of inflamed Leidenfrost drop generation.

This paper aims to broaden the investigation of Leidenfrost drops into the realm of combustion, combining experimental observations and theoretical models to unravel the intricate evaporation mechanics of inflamed Leidenfrost drops. The structure of the paper is as follows. Section II describes the experimental set-up and procedures. Section III compares the lifetimes of inflamed and noninflamed drops. Section IV develops the Leidenfrost case, first discussing existing scalings for standard Leidenfrost drops, then proposing hypotheses for the burning scenario. Here, we derive scalings for lifetime based on initial droplet size and wall temperature, comparing these with experimental data. Section V reports the time evolution of the radii of both inflamed and noninflamed Leidenfrost drops. We first test classical scalings to establish empirical laws, followed by the construction of a dynamic evaporation model in the Leidenfrost state that includes combustion, which we then compare to the ethanol case. Conclusions are drawn in Sec. VI.

II. EXPERIMENTAL SETUP

Figure 2(a) illustrates the experimental setup for capturing images of inflamed drops, comprising a stainless steel substrate, a heating plate (hot plate 1), K-type thermocouples, a high-speed camera (Photron FASTCAM Mini AX200, Camera 1), a digital camera (Sony FDR-AX60, Camera 2), and a 25 W LED cold light source. The mobile nature of Leidenfrost drops forces to trap them or at least to confine them. This was achieved by slightly digging a stainless steel substrate to induce a small curvature. The substrate surface was slightly conical with an angle of approximately 50 mrad which was far enough from conical conditions discussed in Ref. [31]. The substrate's surface roughness R_a was maintained below $0.05 \mu\text{m}$, and its overall diameter was 60 mm, significantly larger than the initial drop radius (less than 6 mm). The wall temperature T_w of the substrate was controlled by the heating plate and the averaged value was calibrated using two K-type thermocouples positioned at the center and edge of the wall. The high-speed camera at 100 frames per second (fps) from a side view, illuminated by the LED cold light source, was used to document the drops whether inflamed or not, measuring the lifetime τ and the shape of the drop. Additionally, the flame of the inflamed drop was captured by the separate digital camera at 25 fps.

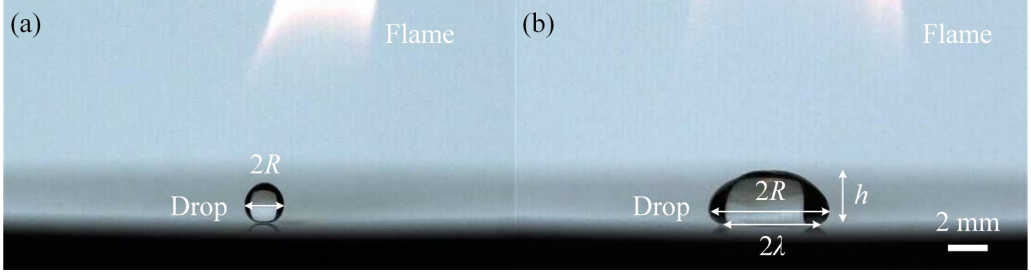


FIG. 3. Shape factors of inflamed Leidenfrost drops (ethanol). (a) Small drops. (b) Large drops. The different shape factors are reported in the figures.

The preparation of inflamed drops varied depending on the wall temperature T_w relative to the Leidenfrost temperature T_{Leid} . For $T_w < T_{Leid}$, drops were gently released onto the micro-conical stainless steel substrate heated to the target temperature by hot plate 1 and quickly ignited with a flame. In contrast, for $T_w > T_{Leid}$, a different procedure was employed to study the evaporation of a burning drop, as depicted in Fig. 2(b). A predefined volume of liquid was drawn into a micropipette from a glass tube and precisely dispensed into a container preheated to 250 °C (using another hot plate, referred to as hot plate 2), exceeding T_{Leid} to induce the Leidenfrost state. The resulting Leidenfrost drop was then promptly ignited and transferred onto the substrate, which was maintained at the target temperature by hot plate 1. Figure 3 presents typical examples of small and large inflamed Leidenfrost drops, categorized by their capillary lengths $l_c = \sqrt{\sigma_l / \rho_l g}$ (approximately 1.6 mm for ethanol, where σ_l , ρ_l and g are the surface tension of the liquid, the density of the liquid and the acceleration of the gravity respectively). Our analysis focused primarily on the lateral expansion R (i.e., radius; R_0 being the initial radial expansion) of the Leidenfrost drop, with other geometric parameters such as height h and bottom contact radius λ derived from models like that proposed in [32,33]. The experiments utilized ethanol (99.8%, [vol/vol]) and n-heptane (98.5%, [vol/vol]) as liquid fuels, along with a water-ethanol mixture (20%-80%, [vol/vol]) to investigate anomalies in the lifetime-temperature relationship (see Fig. 6). The physical properties of these liquids, including boiling point T_b (°C), surface tension σ_l (mN · m⁻¹), density ρ_l (kg · m⁻³), viscosity μ_l (mPa · s), capillary length l_c (mm), and latent heat of evaporation ΔH_v (J · g⁻¹), are summarized in Table I, with data sourced from Lemmon *et al.* [34] and Ref. [35]. Prior to each experiment, the substrate was cleaned in an ultrasonic cleaner for 10 minutes to remove contaminants, and a blower eliminated any adsorbed dust particles, ensuring experimental accuracy. The measurement uncertainties for length and temperature were 42.6 μm/pixel and 1 °C.

III. INFLAMED DROPS

Once inflamed, the droplet was released on the controlled-temperature substrate on which the lifetime of the droplet was measured. In Fig. 4, we compare in a semi-log plot the drop lifetime τ against the wall temperature T_w for ethanol and n-heptane drops with the same initial volume of $V_0 = 240 \pm 5$ μL, where the noninflamed and inflamed states denote τ_{ni} and τ_i , respectively. The

TABLE I. Physical properties of different liquids at the boiling point.

Liquids	T_b (°C)	σ_l (mN/m)	ρ_l (kg/m ³)	μ_l (mPa.s)	l_c (mm)	ΔH_v (J/g)
ethanol	78.3	18.6	750	0.420	1.6	838
80% ethanol	79.8	21.3	805	0.563	1.7	
n-heptane	98.0	12.7	614	0.197	1.5	317

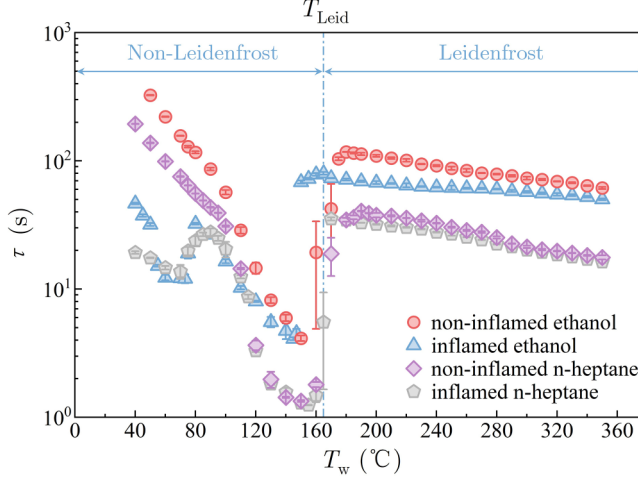


FIG. 4. The drop lifetime τ as a function of wall temperature T_w for different evaporating drops. T_w ranged from 40 °C to 350 °C. The drop entered the Leidenfrost regime when $T_w \geq T_{\text{Leid}}$. The diagram, with an example of inflamed ethanol drops, shows the Leidenfrost and non-Leidenfrost regions ($T_{\text{Leid}} = 165$ °C).

lifetime curve of noninflamed drops, similar to water drops, has been widely reported in previous studies [7,9]. In essence, the lifetime τ_{ni} decreases as the temperature of the wall increases. A minimum is reached that corresponds to the maximum of heat transfer. Then, for a slight increase of the temperature, the lifetime sharply increases while the Leidenfrost state establishes. The Leidenfrost temperatures T_{Leid} are found to be 180 °C for noninflamed ethanol and 190 °C for noninflamed n-heptane.

The general aspect of the inflamed drop lifetime τ_i is pretty similar to the noninflamed case. Taking inflamed ethanol drops as an example, we distinguish in Fig. 4: non-Leidenfrost and Leidenfrost states. First, the Leidenfrost temperature T_{Leid} slightly decreases due to the presence of the flame (165 °C for inflamed ethanol and 170 °C for inflamed n-heptane). Second, a bump below the Leidenfrost transition occurs around 80 °C for both liquids. Third, the difference between the lifetime of noninflamed and inflamed Leidenfrost drops decreases with increasing T_w until 350 °C, which shows that the inflamed drop lifetime τ_i is less and less influenced by the flame when $T_w \gg T_{\text{Leid}}$.

A. Evaporation modes

According to the wall temperature, different evaporation behaviors can be observed. We present a detailed illustration of the evaporation modes of inflamed drops on a hot substrate. Taking ethanol as an example, we identify four distinct evaporation modes, delineated by three characteristic temperatures (blue dotted lines) in Fig. 5: $T_b \sim 80$ °C (approximately the saturation temperature), $T_c = 147$ °C (critical heat flux temperature), and $T_{\text{Leid}} = 165$ °C (Leidenfrost temperature). A typical picture of each mode is reported in Fig. 6, including schematic representations of drop shapes in the considered mode. Additionally, the flame development and the duration of the burning process can be observed in Movie S1 in the Supplemental Material (SM) [36].

In Mode I ($T_w < 80$ °C), the evaporation of the burning drop accelerates significantly, leading to an expanded spread area and intense flame due to the substrate's favorable wettability [see $T_w = 70$ °C in Fig. 6(a)], where burning dominates the drop's lifetime. The flame is high due to the large spreading of the droplet.

In Mode II (80 °C $\leq T_w \leq 147$ °C), a bump is observed in the lifetime as a function of the wall temperature. The bottom of the drop undergoes rapid heat exchange with the substrate as T_w exceeds

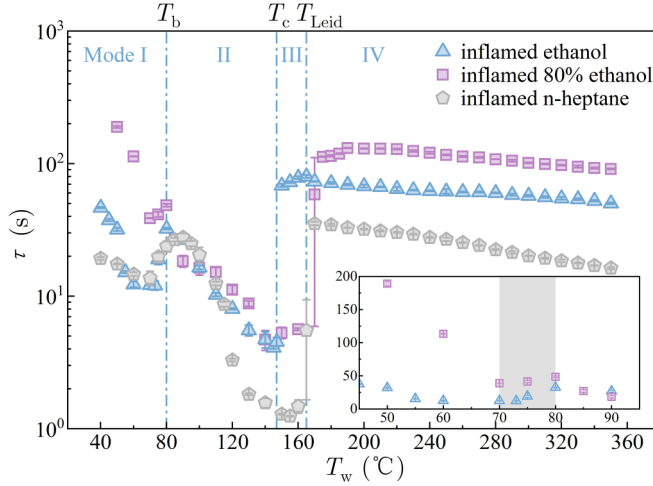


FIG. 5. The lifetime τ as a function of wall temperature T_w for different inflamed drops ($V_0 = 240 \pm 5 \mu\text{L}$). Using inflamed ethanol drops as an example, the four distinct evaporation modes (I–IV) are presented by vertical dotted lines corresponding to the three characteristic temperatures: $T_b \sim 80^\circ\text{C}$, $T_c = 147^\circ\text{C}$, and $T_{\text{Leid}} = 165^\circ\text{C}$. The inset shows the comparison of the lifetimes of inflamed ethanol and inflamed 80% ethanol drops in the abnormal temperature ranges ($70^\circ\text{C} \sim 80^\circ\text{C}$).

the boiling point of ethanol, resulting in the formation of numerous small bubbles at the solid-liquid interface and initiating nuclear boiling [see $T_w = 90^\circ\text{C}$ in Fig. 6(b)]. As T_w increases, a higher number of boiling bubbles rises [see $T_w = 130^\circ\text{C}$ in Fig. 6(b)], further intensifying the flame. Both burning and nonburning ethanol drops exhibit the same lifetime ($\tau \sim 4.50$ s) at $T_w = 147^\circ\text{C}$ (see Fig. 4), indicating a transition in the dominant evaporation mode from burning to boiling.

In Mode III ($147^\circ\text{C} < T_w < 165^\circ\text{C}$), the rapid coalescence of microbubbles promotes the formation of a vapor cushion, enabling the burning drop to levitate. However, this vapor layer lacks stability (pre-Leidenfrost regime), making the drop susceptible to wall contact, which could lead to

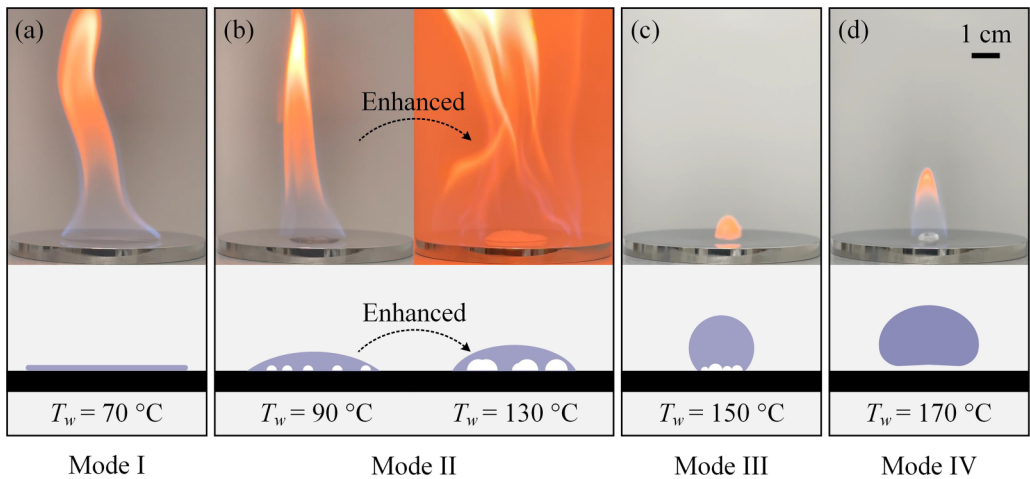


FIG. 6. The evaporation mode of inflamed ethanol drops on a hot substrate. (a) Mode I: Burning. (b) Mode II: Boiling. (c) Mode I: Burning-boiling. (d) Mode I: Burning-Leidenfrost. Each figure includes a flame snapshot (top) and a corresponding schematic diagram of the drop shape during combustion (bottom).

a boiling-induced explosion, as observed at $T_w = 150^\circ\text{C}$ in Fig. 6(c). Notably, at $T_w = 160^\circ\text{C}$, the burning drop surpasses the nonburning case in lifetime (refer to Fig. 4), demonstrating a synergistic effect of burning and boiling on drop evaporation. The consequence is the decrease of the Leidenfrost temperature compared to the noninflamed case.

In Mode IV ($T_w \geq 165^\circ\text{C}$), the drop reaches a stable Leidenfrost state, significantly extending its lifetime and reducing flame size compared to the burning or nucleate boiling-dominated modes (I and II). This is evident when comparing the burning-Leidenfrost and burning-boiling drops at $T_w = 170^\circ\text{C}$ and $T_w = 130^\circ\text{C}$, respectively, in Fig. 6. The difference in lifetime between nonburning and burning Leidenfrost drops decreases as T_w increases, reaching up to 350°C . These results highlight the interplay between burning and the Leidenfrost effect in determining drop longevity, with combustion in the Leidenfrost state significantly prolonging burning time compared to lower temperature cases. Additionally, the nearly spherical morphology of the drop during evaporation minimizes the surface area available for combustion, optimizing the utilization of the liquid volume.

B. Lifetime anomaly below Leidenfrost temperature

To explore the origin of the bump in Mode II, a mixture composed of 20% water and 80% ethanol was tested. The lifetime of this mixture is reported in Fig. 5 (square symbols), where the bump is significantly suppressed (see the inset). Figure 5 also shows a zoom of the evaporation time τ as a function of the wall temperature T_w for three types of inflamed drops: ethanol (triangle), 80% ethanol (square), and n-heptane (pentagon), which is an extension of Fig. 4. The Leidenfrost temperature T_{Leid} is the highest for the mixture, reaching 190°C for inflamed 80% ethanol because of the presence of water. The water content has three impacts on the lifetime of the droplet. The first was to increase the Leidenfrost temperature. The second was to increase the lifetime at any given temperature. The third was to change the nuclear boiling mode. As water and ethanol are expelled from the droplet, the combustion has less influence on the lifetime compared to pure ethanol case.

IV. INFLAMED DROPS IN LEIDENFROST STATE

In this section, we first recall the scaling of noninflamed Leidenfrost drops based on Baumeister's work. Afterwards, we discuss the observations of inflamed Leidenfrost drops and the assumptions underlying the inflamed Leidenfrost mechanism. By separating the evaporation contributions from the top and bottom, we report the lifetime as a function of the initial drop radius at a fixed wall temperature of 300°C . Next, we show the lifetime dependence on the wall temperature for specific initial droplet radii. These observations allow to elaborate a model for the evaporation of inflamed drops over time.

A. Classical scaling of noninflamed Leidenfrost drops

Previous studies [37] have revealed that the evaporation dynamics of a Leidenfrost drop on a hot substrate are primarily influenced by the initial drop size R_0 (see Movie S2 in the SM [36]) and the wall temperature T_w . The lifetime τ_{ni} of a noninflamed Leidenfrost drop follows power laws with respect to both R_0 and the temperature difference ΔT (so-called superheat) between the substrate temperature T_w and the liquid boiling temperature T_b . Specifically, we have $\tau_{\text{ni}} \sim R_0^\alpha \Delta T^\beta$, where the exponents α and β depend solely on R_0 relative to the capillary length l_c .

Here, we adopt the scaling derived by Baumeister *et al.* [33,38], where heat transfer is computed by considering the speed of the vapor generated perpendicular to the substrate. For the noninflamed Leidenfrost drop on a hot substrate, according to the scaling found in Ref. [33], the lifetime dependence on R_0 and ΔT are given by

$$\tau_{\text{ni}} \sim R_0^{2/3} \Delta T^{-3/4} \quad \text{for } R_0 > l_c, \quad (1)$$

$$\tau_{\text{ni}} \sim R_0^{5/4} \Delta T^{-3/4} \quad \text{for } R_0 < l_c. \quad (2)$$

B. Observations and assumptions

In the Leidenfrost state, the liquid does not boil even during combustion, which means that the temperature within the Leidenfrost drop remains below its boiling temperature. This particular observation indicates that the presence of a flame does not modify the thermal and geometrical conditions for the bottom part of the Leidenfrost drop. Even if the vapor produced between the drop and the wall is inflamed, it does not influence the gas generation originated from the bottom of the drop. On the other hand, when inflamed, the flame works at the top of the drop, necessitating consideration of evaporation at this location. Notably, the adiabatic temperature of a flame surpasses 1000 °C (e.g., 1362 °C for ethanol [39]). Consequently, the top contribution of drop evaporation cannot be disregarded. In essence, while the drop evaporation at the bottom remains independent of the top, the top evaporation becomes significant when inflamed.

We assume that the bottom evaporation of an inflamed Leidenfrost drop can still be modeled akin to a classical Leidenfrost drop because the temperature field close to the developed vapor film is not influenced by the flame. Meanwhile, the top evaporation cannot be *a priori* thought to be independent of the evaporation that occurs at the bottom of the inflamed Leidenfrost drop since the vapor produced at the lower part feeds the flame. However, as a first step (we will verify *a posteriori* whether this hypothesis holds), we assume that the lifetime of the drop can be thought to be the sum of the contributions from the bottom (known from the noninflamed case) and the top (due to combustion). We split the problem into the bottom and top parts. In so doing, the total mean evaporation rate of an inflamed Leidenfrost drop, denoted as \dot{m}_i , is the sum of mass flow rates from both parts: $\dot{m}_i = \dot{m}_- + \dot{m}_+$, where \dot{m}_+ refers to the top and \dot{m}_- to the bottom. We have access to the lifetimes τ_{ni} for the noninflamed drop and τ_i for the inflamed drop, along with the initial mass m_0 of the drop. The total mean evaporation rate (i.e., the total mass flow rate) is then given by $\dot{m}_i = m_0/\tau_i$. The bottom evaporation contribution \dot{m}_- is estimated under the assumption that it equals the total mean evaporation rate of a noninflamed drop: $\dot{m}_- = \dot{m}_{ni} = m_0/\tau_{ni}$. Finally, the evaporation contribution of the top part \dot{m}_+ and its characteristic lifetime τ_+ are deduced by subtraction: $\dot{m}_+ = \dot{m}_i - \dot{m}_{ni} = m_0(1/\tau_i - 1/\tau_{ni})$.

C. Inflamed Leidenfrost drops: Radius scaling

In Fig. 7(a), we present the measured lifetimes (τ_{ni} and τ_i) of noninflamed (red circle for ethanol and purple diamond for n-heptane) and inflamed (blue triangle for ethanol and gray pentagon for n-heptane) Leidenfrost drops across various initial radius R_0 on a hot substrate at a fixed temperature of 300 °C ($\approx 2T_{Leid}$). The closed and open symbols refer to R_0 larger or smaller than l_c respectively. Indeed, a transition in regimes occurs around $R_0 \approx l_c$. For large ethanol drops, the fitting exponent α is approximately 0.65 ~ 0.67 ($\approx 2/3$), whereas, for small ethanol drops, α is approximately 1.21 ~ 1.24 ($\approx 5/4$). Interestingly, the exponent remains relatively unaffected by whether the ethanol drop is inflamed, except for extremely small radii. This observation is further validated through experimental data on noninflamed and inflamed n-heptane Leidenfrost drops, with fitting exponents $\alpha = 0.65 \sim 0.72$ ($\approx 2/3$) for large drops and 1.22 ~ 1.26 ($\approx 5/4$) for small drops. These experimentally derived exponents closely align with the theoretical scalings in Eqs. (1) and (2). However, the distinction between inflamed and noninflamed cases lies in the absolute values of the lifetimes (see Movie S2 in the SM [36]).

Figure 7(b) presents the ratio \dot{m}_-/\dot{m}_+ of the average evaporation rates at the top to the bottom as a function of the initial radius R_0 for $T_w = 300$ °C. Remarkably, regardless the nature of the liquid, $\dot{m}_- > \dot{m}_+$. That is, the evaporation contribution from the bottom part is always larger whatever the size of the drop. The ratio \dot{m}_-/\dot{m}_+ increases with R_0 until $R_0 \simeq l_c$. Then it remains constant ($\dot{m}_-/\dot{m}_+ \approx 5$) for a large range of radii for ethanol. However, for n-heptane, it increases to reach another plateau ($\dot{m}_-/\dot{m}_+ \approx 10$) when $R_0 > 3$ mm. Actually, this can be explained by the star-shaped oscillations of the n-heptane droplet when $R_0 > 2l_c$ due to the influence of the bottom capillary wave [40]. In this case, the fast upward airflow around the inflamed n-heptane drop (high evaporation

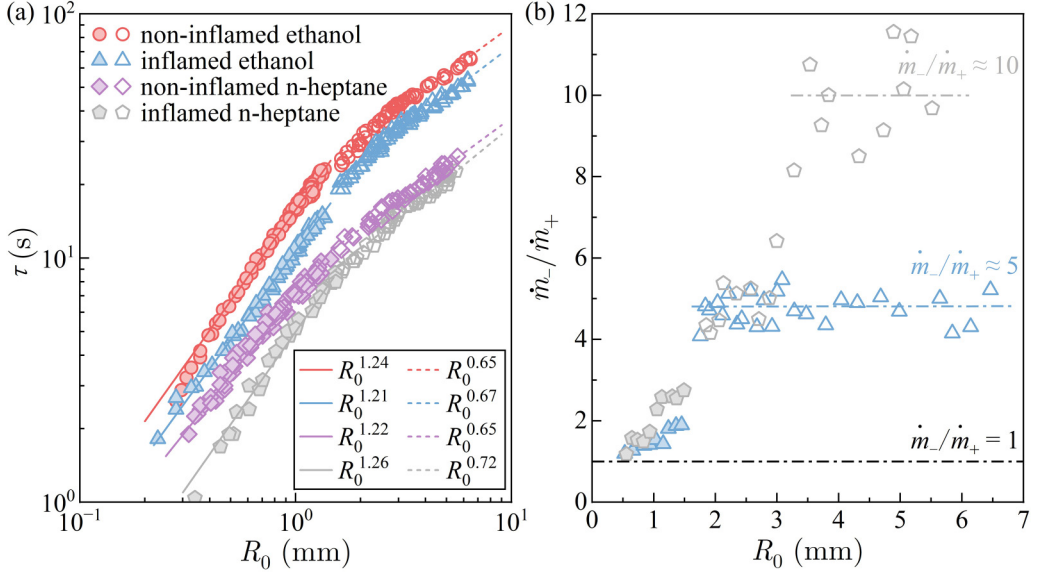


FIG. 7. (a) The measured lifetimes τ of noninflamed and inflamed Leidenfrost drops as a function of the initial radius R_0 at $T_w = 300^\circ\text{C}$. Straight lines indicate power law fits (see legend). Different shaped symbols represent various cases (noninflamed/flamed and ethanol/n-heptane). Open and closed symbols denote large and small drops, respectively. (b) The ratio \dot{m}_-/\dot{m}_+ of the mass flow rate of the bottom to the top of an inflamed Leidenfrost drop as a function of the initial drop radius R_0 at $T_w = 300^\circ\text{C}$. The evaporation contributions from the bottom \dot{m}_- and the top \dot{m}_+ are deduced from drop lifetimes without and with flame (see text). Symbols of the same shape in (a) and (b) correspond to the same legend.

rate) and incomplete combustion (observed as a large amount of black smoke around the n-heptane flame in the experiment while ethanol flame did not) result in weak heat transfer from the flame to the n-heptane drop at the top. The plateau finds for large drops ($R_0 > l_c$) demonstrates that both the evaporation contributions from the top and bottom follow a same scaling regarding R_0 . When the volume is large, the Leidenfrost drop shape is assimilated to a cylinder with a thickness equals to $2l_c$ [7]. As a consequence, increasing the drop initial volume enhances the evaporation surface area of both the top and bottom parts equally. At first approximation, the heat exchange with the hot substrate is proportional to the surface area, and so is the same for the inflamed part of the Leidenfrost drop. However, the physical description is more complex for small drops, as demonstrated in previous studies, such as Ref. [41], which focused on noninflamed drops. Thus, the ratio \dot{m}_-/\dot{m}_+ depends on R_0 and the splitting between top and bottom evaporation is not obvious.

D. Inflamed Leidenfrost drops: Temperature scaling

The temperature scaling is obtained in the same procedure as the radius scaling. Figure 8 illustrates the dependence of the mass flow rate \dot{m} (the specific contribution is reported in the legend) on superheat ΔT for inflamed ethanol and n-heptane Leidenfrost drops with initial radii R_0 of 1.1 mm and 3.1 mm, respectively. Each plot includes the total mass flow rate \dot{m}_i , the bottom contribution \dot{m}_- (equal to \dot{m}_{ni}), and the top contribution \dot{m}_+ , all as functions of ΔT for inflamed Leidenfrost drops. Whether the drops are small ($R_0 = 1.1$ mm) and large ($R_0 = 3.1$ mm), or ethanol and n-heptane, the trend in the experimental data closely resembles. Both the total mass flow rate \dot{m}_i and the bottom contribution \dot{m}_- can be fitted as power laws, and the bottom contribution dominates over the top contribution. The top contribution \dot{m}_+ remains nearly constant

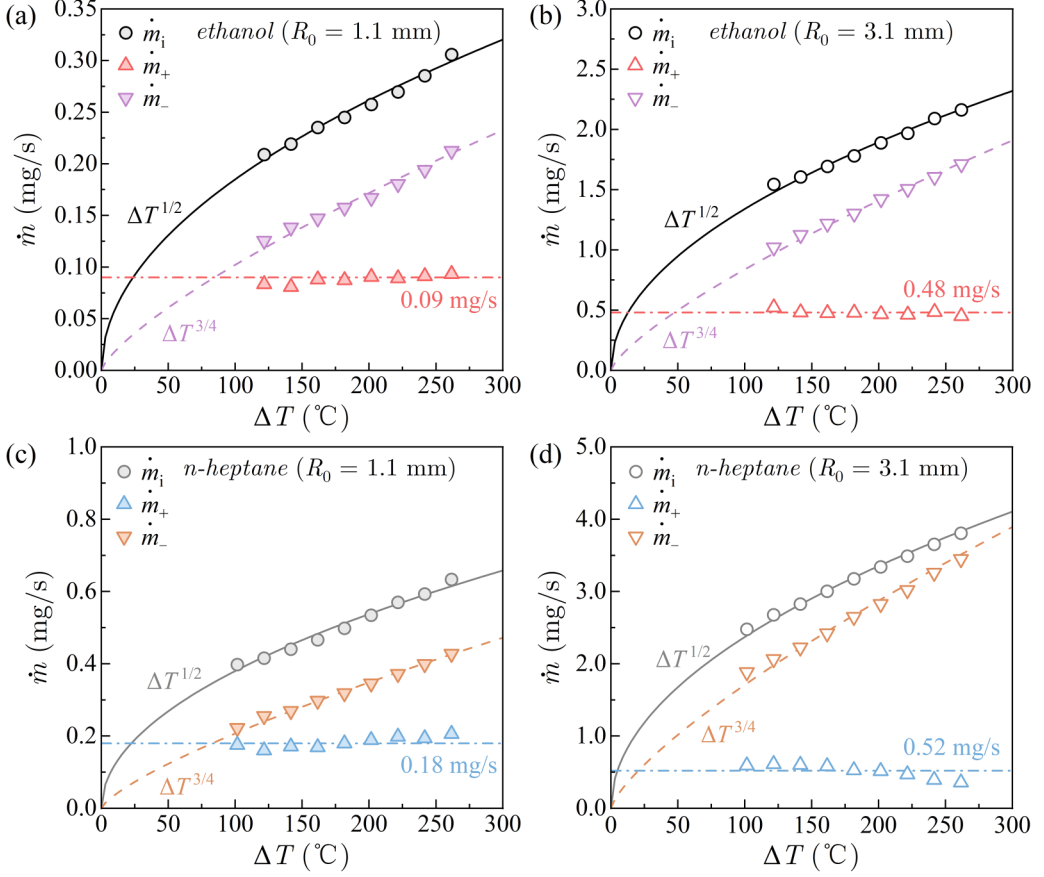


FIG. 8. (a), (b) Dependence of the mass flow rate \dot{m} as a function of the superheat ΔT for inflamed ethanol Leidenfrost drops in (a) $R_0 = 1.1$ mm and in (b) $R_0 = 3.1$ mm. (c), (d) Dependence of the mass flow rate \dot{m} as a function of the superheat ΔT for inflamed n-heptane Leidenfrost drops in (c) $R_0 = 1.1$ mm and in (d) $R_0 = 3.1$ mm. \dot{m}_i , \dot{m}_- and \dot{m}_+ are the total mass flow rate, the bottom contribution and the top contribution, respectively.

across the wall temperature range considered. However, some variations are observed compared to the ethanol case, attributed to oscillations in a star-shape experienced by large n-heptane Leidenfrost drops.

The presence of a flame significantly increases the total mass flow rate \dot{m}_i . Power laws were fitted and were found to scale alike $\Delta T^{1/2}$ for inflamed drops. On the other hand, irrespective of the initial size of the drop, the bottom contribution \dot{m}_- (i.e., the mass flow rate of the noninflamed drop) was successfully fitted by $\Delta T^{3/4}$, in line with predictions from Ref. [33]. The so-computed top contribution \dot{m}_+ is found to be constant (0.09 mg/s and 0.48 mg/s for ethanol, and 0.18 mg/s and 0.52 mg/s for n-heptane) in the range of considered wall temperatures ($\Delta T = 122$ °C \sim 272 °C). These observations both hold for ethanol and n-heptane. Therefore, we can conclude that the temperature scaling is contingent upon the presence of a flame but is essentially unaffected by the size and nature of the drop. Moreover, the bottom contribution is found to be always larger (up to five times) than the top contribution. Consequently, the found scaling $\dot{m}_i \propto \Delta T^{1/2}$ cannot be considered as a scaling law since it results from the sum of two comparable contributions.

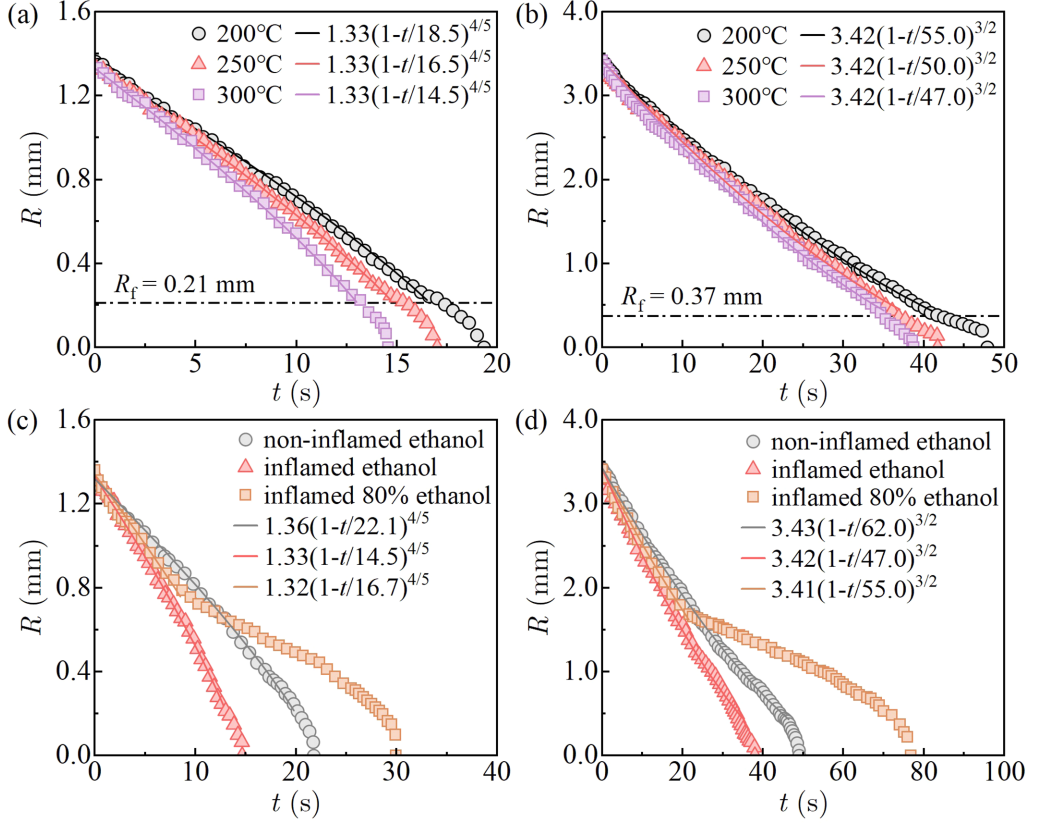


FIG. 9. (a), (b) Time evolution of the radius of the inflamed ethanol Leidenfrost drop at various wall temperatures. Three cases: 200 °C (black circles), 250 °C (red triangles), 300 °C (purple squares) for small drops ($R_0 = 1.33$ mm) in (a) and large drops ($R_0 = 3.42$ mm) in (b). (c), (d) Time evolution of the radius of the Leidenfrost drop in various evaporation states. Three types: noninflamed ethanol (gray circles), inflamed ethanol (red triangles), inflamed 80% ethanol (brown squares) for small drops ($R_0 = 1.32 \sim 1.36$ mm) in (c) and large drops ($R_0 = 3.41 \sim 3.43$ mm) in (d). All fitting lines in (a)–(d) are limited to the ethanol evaporation stage and based on Eq. (3).

V. TIME EVOLUTION OF THE RADIUS

A. Confrontation to classical scalings

Figures 9(a)–9(b) depicts the time evolution of the radius of inflamed ethanol Leidenfrost drops at three distinct wall temperatures: 200 °C, 250 °C, and 300 °C. The initial radii R_0 for small and large drops were 1.33 mm and 3.42 mm, respectively. The presence of a flame persisted until the critical radius R_f reached 0.21 mm and 0.37 mm, respectively. Once $R < R_f$, the ethanol component within the drop is largely consumed, transitioning to a nonflame stage, where evaporation is driven primarily by the noncombustible component (predominantly water) until the drop is completely vaporized. Notably, the critical radius R_f is dependent upon the absolute volume of the noncombustible component in the initial drop, owing to variations in water content arising from the impure ethanol. According to the relations between the lifetimes of large and small Leidenfrost drops in Eqs. (1) and (2), and the boundary conditions (i.e., $R = R_0$ when $t = 0$ and $R = 0$ when $t = t^*$, where t^* is the theoretical lifetime of a pure ethanol drop without other components), we can determine the

time-dependent drop radius R during evaporation [33,37]:

$$R = \begin{cases} R_0(1 - t/t^*)^{4/5} & \text{when } R_0 < l_c \\ R_0(1 - t/t^*)^{3/2} & \text{when } R_0 > l_c \end{cases} \quad (3)$$

Theoretical curves described by Eq. (3) align well with the experimental data obtained from inflamed ethanol Leidenfrost drops during the flame stage ($R > R_f$).

Figures 9(c) and 9(d) further show the time evolution of the radius of Leidenfrost drops under three different evaporation states: noninflamed ethanol, inflamed ethanol, and inflamed 80% ethanol, at $T_w = 250^\circ\text{C}$. The initial radii R_0 for small and large drops ranged $1.32 \sim 1.36$ mm and $3.41 \sim 3.43$ mm, respectively. During the flame stage ($R > R_f$), similar fitting lines based on the scaling laws in Eq. (3) were observed in different Leidenfrost drops. A regime transition is evident in the large Leidenfrost drop. The inflamed ethanol case corresponds to that discussed in Figs. 9(a) and 9(b), while the radius decrease of the inflamed 80% ethanol drop follows the behavior of the inflamed (99.8%) ethanol drop during the flame stage. After the ethanol is burnt out, the water continues to evaporate in the nonflame stage ($R < R_f$). Remarkably, the final lifetime of the inflamed 80% ethanol drop ($\tau = 30.0$ s) is twice that of the inflamed ethanol drop ($\tau = 14.7$ s).

These investigations show that Eq. (3) provides an interesting scaling law to report the time evolution of the radius. However, the value of t^* remains difficult to apprehend. An explicit time evolution of the radius can be obtained by resolving the model proposed in Ref. [33].

B. Evaporation model of inflamed Leidenfrost drops

In summary, regarding the results of the mass flow rate measurements according to the initial radius and to the superheat, we can conclude that the decoupling between the top and bottom contributions is well established for large Leidenfrost drops ($R_0 > l_c$). The bottom contribution is independent of the top because the geometry and the local thermal environment near the bottom vapor film stay the same with or without the presence of the flame. One can only suppose that the top contribution is decoupled from the bottom for a similar reason: the flame generated constitutes a thermal environment that remains stable in the range of considered parameters.

The decoupling is less obvious for small drops and low superheat, since the contributions are sensitively equal and the mass transfer ratio (bottom/top) depends on the radius [see Fig. 7(b)]. Let us also remind that the flame was observed to disappear when the droplet becomes tiny. Finally, we can evaluate the burning rate per unit surface ϕ by dividing \dot{m}_+ by πR_0^2 , and find $23 \text{ g/m}^2 \cdot \text{s}$ at $R_0 = 1.1$ mm (small drop) and $16 \text{ g/m}^2 \cdot \text{s}$ at $R_0 = 3.1$ mm (large drop) in the case of ethanol. Moreover, from Fig. 7, we observe that the ratio of mass flow rates is more stable in the case of ethanol (see discussion above). In the following, we focus on the case of ethanol.

In the context of the large drop approximation, the evaporation process of the bottom part can be described as outlined in Ref. [33]. In this framework, the droplet shape is a cylinder of volume V (the volume of the droplet) and of section A that depends on the volume. The heat is transferred via conduction through the vapor film. More specifically, volume variation \dot{V}_- is deduced from the energy balance. The heat transferred to the droplet by conduction through the vapor film converts the water into vapor:

$$\Delta H_v \rho_l \dot{V}_- = f^{-1} h_v(V) A(V) \Delta T, \quad (4)$$

where ΔH_v , ρ_l , $h_v(V)$, $A(V)$, and f are the latent heat of evaporation, the density of the liquid, the heat transfer coefficient, the heat transfer area of the bottom face of the droplet, and the radiation correction factor, respectively. The heat transfer coefficient h_v and the bottom heat transfer area A of Leidenfrost drops are explicit functions of the volume V . The evaluation of $h_v(V)$ and $A(V)$ are given in Ref. [33] for different size of the droplet. Here, we report on the case of large drops relevant

to the present study. The relations are given by

$$h_v(V) = 1.075 \left(\frac{k_v^3 \Delta H_v^* g^{1/2} \rho_l^{1/2} \rho_v \sigma_l^{1/2}}{\mu_v \Delta T V^{2/3}} \right)^{1/4} \quad (5)$$

and

$$A(V) = 1.25 \left(\frac{\sigma_l}{\rho_l g} \right)^{-1/4} V^{5/6}, \quad (6)$$

where the modified heat of evaporation is

$$\Delta H_v^* = \Delta H_v \left(1 + \frac{7c_p \Delta T}{20 \Delta H_v} \right)^{-3} \quad (7)$$

and c_p is the specific heat of the liquid, μ_v , ρ_v , k_v , ΔH_v , σ_l , and g are the viscosity, density, and thermal conductivity of the vapor, the latent heat of evaporation, the surface tension of the drop, and the acceleration of gravity. The resolution of this system, using a Python procedure from the SciPy package, specifically the `solve_ivp` function with the implicit Runge-Kutta method and a time step of 5 ms, allows to obtain $V(t)$ and then $R(t)$ through Eq. (6):

$$R = \sqrt{\frac{1.25(\sigma_l/(\rho_l g))^{-1/4} V^{5/6}}{\pi}}, \quad (8)$$

which considers that the drop is a cylinder with section A (i.e., $A = \pi R^2$). This model was used to fit the data $R(t)$ of noninflamed drop, which allows to obtain the factor f of radiative correction [see Eq. (4)].

Then, to account for the inflamed drop, we introduce an additional combustion term, i.e., the top evaporation contribution \dot{V}_+ . Indeed, this term is modeled to be proportional to the area $A(V)$ (the surface of the bottom and of the top are supposed to be equal)

$$\dot{V}_+ = A(V)\phi. \quad (9)$$

The total mean evaporation rate is the sum of the contributions from the top and the bottom

$$\dot{V} = \dot{V}_- + \dot{V}_+. \quad (10)$$

In Fig. 10, we compare the evolution of the radius as a function of time for both noninflamed and inflamed ethanol Leidenfrost drop. Equation (4) was implemented according to the physical parameters of ethanol to obtain the theoretical evolution of the radius as a function of time for noninflamed drops (see black solid curve). There was only one parameter of calibration that accounts for the radiation correction $f(=0.45)$ in the transmission of the heat from the wall to the drop. Then, Eq. (10) was implemented to deduce the theoretical variation of the radius for the inflamed drop (see purple solid curve). The burning rate per unit surface area ϕ is obtained by dividing the total evaporation rate [$16 \text{ g/m}^2 \cdot \text{s}$ from Fig. 8(b)] by the heat transfer area. Overall, the agreement with the observation is satisfactory regarding the different simplifications of the model. The lifetime of the inflamed Leidenfrost drop can be deduced from the model according to an arbitrary cut-off value of the radius R_c . Here, we took $R_c = l_c$ (change of regime towards small drops). The so-computed lifetimes $\tau(R_c = l_c)$ (purple squares) are plotted against the superheat ΔT in the inset. They are compared to the experimental lifetimes (black circles). The dashed lines correspond to fit by power law in $\Delta T^{-1/2}$. This semi-empirical law is comparable to the scaling found in Fig. 8 for the dependence of the mass flow rate with the temperature. It is important to note that the model underestimates the experimental data because of the radius cut-off. Again, the power law we found has no physical origin since the data clearly indicate that the lifetime is the sum of two contributions.

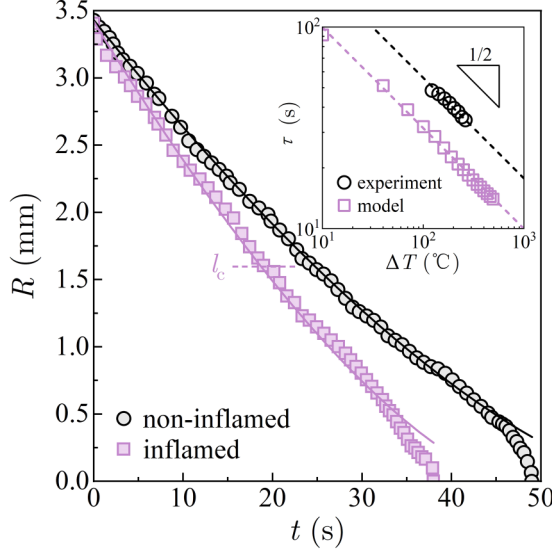


FIG. 10. The decrease of the radius R of the noninflamed and inflamed ethanol Leidenfrost drop is presented as a function of time t with $R_0 = 3.4$ mm and $T_w = 300$ °C. The black and purple solid curves are deduced by Eqs. (4) and (10), respectively. In the inset, the experimental and model lifetimes τ of inflamed ethanol Leidenfrost drops are compared as a function of the superheat ΔT at $R_c = l_c$. The black and purple dashed curves are deduced from the power law of $\tau \propto \Delta T^{-1/2}$.

VI. CONCLUSION

Our findings reveal that an inflamed drop in the Leidenfrost state exhibits prolonged lifetime and high mobility. This extended lifetime, allowing the flame to endure for an extended period with the same amount of fuel, poses a significant challenge for fire suppression efforts compared to a sessile drop. Our study underscores the importance of controlling the Leidenfrost temperature relative to the substrate, as it has implications for heat transfer and fire suppression strategies. Through our experiments, we successfully separated the contributions to drop evaporation from both the top and bottom parts. Despite the flame's higher temperature compared to the substrate, we demonstrated that evaporation at the bottom of the drop predominates over that at the top, particularly for drops larger than the capillary length. This holds significant implications for comprehensively understanding the interaction between burning drops and hot wall surfaces, as well as for efficiently utilizing energy in a Leidenfrost state. Moreover, an inflamed Leidenfrost drop offers an alternative means to measure the intrinsic burning rate of a flammable liquid. Direct measurement of this burning rate is challenging due to factors such as the presence of the burning pool's border [42] or the porosity of an inflamed solid sphere fed with liquid [43]. The analysis of the top contribution allows to determine an order of magnitude of the burning rate without considering border problem. Indeed, in the large Leidenfrost drop regime, the pool border essentially is the drop itself. Thus, the evaporation rate at the top is an intrinsic reflection of the liquid's burning rate at its saturated temperature. The observed top evaporation of inflamed Leidenfrost drops is comparable to laminar convection heat transfer seen in pool fires with small pool diameters (<0.05 m) [42].

ACKNOWLEDGMENTS

This research was supported by “Pioneer” and “Leading Goose” R&D Program of Zhejiang [Grant No. 2024C03279(SD2)] and the Ningbo Key Research and Development Program (Grants

No. 2024Z178 and No. 2023Z038). S. Dorbolo thanks F.R.S.-FNRS for financial support as a Senior Research Associate.

DATA AVAILABILITY

The data that support the findings of this article are openly available [44].

-
- [1] D. Zang, S. Tarafdar, Y. Y. Tarasevich, M. D. Choudhury, and T. Dutta, Evaporation of a droplet: From physics to applications, *Phys. Rep.* **804**, 1 (2019).
 - [2] E. Krepper, B. Končar, and Y. Egorov, Cfd modelling of subcooled boiling—concept, validation and application to fuel assembly design, *Nucl. Eng. Des.* **237**, 716 (2007).
 - [3] P. Calvert, Inkjet printing for materials and devices, *Chem. Mater.* **13**, 3299 (2001).
 - [4] Y. Zhao, S. Kuang, X. Zhang, and M. Xu, Experimental investigation on the dynamics of a single water droplet impacting wood surface, *Exp. Therm Fluid Sci.* **151**, 111094 (2024).
 - [5] A. C. Siegel, S. T. Phillips, M. D. Dickey, N. Lu, Z. Suo, and G. M. Whitesides, Foldable printed circuit boards on paper substrates, *Adv. Funct. Mater.* **20**, 28 (2010).
 - [6] D. F. Hanks, Z. Lu, J. Sircar, T. R. Salamon, D. S. Antao, K. R. Bagnall, B. Barabadi, and E. N. Wang, Nanoporous membrane device for ultra high heat flux thermal management, *Microsyst. Nanoeng.* **4**, 1 (2018).
 - [7] D. Quéré, Leidenfrost dynamics, *Annu. Rev. Fluid Mech.* **45**, 197 (2013).
 - [8] J. C. Burton, A. L. Sharpe, R. C. A. Van Der Veen, A. Franco, and S. R. Nagel, Geometry of the vapor layer under a leidenfrost drop, *Phys. Rev. Lett.* **109**, 074301 (2012).
 - [9] G. Liang and I. Mudawar, Review of drop impact on heated walls, *Int. J. Heat Mass Transf.* **106**, 103 (2017).
 - [10] J. G. Leidenfrost, On the fixation of water in diverse fire, *Int. J. Heat Mass Transf.* **9**, 1153 (1966).
 - [11] C. Kleinstreuer and Z. Zhang, Airflow and particle transport in the human respiratory system, *Annu. Rev. Fluid Mech.* **42**, 301 (2010).
 - [12] M. Liu, J. Li, X. Zhou, J. Li, S. Feng, Y. Cheng, S. Wang, and Z. Wang, Inhibiting random droplet motion on hot surfaces by engineering symmetry-breaking janus-mushroom structure, *Adv. Mater.* **32**, 1907999 (2020).
 - [13] I. U. Vakarelski, J. O. Marston, D. Y. C. Chan, and S. T. Thoroddsen, Drag reduction by leidenfrost vapor layers, *Phys. Rev. Lett.* **106**, 214501 (2011).
 - [14] H. A. Stone, A. D. Stroock, and A. Ajdari, Engineering flows in small devices: Microfluidics toward a lab-on-a-chip, *Annu. Rev. Fluid Mech.* **36**, 381 (2004).
 - [15] M. Adda-Bedia, S. Kumar, F. Lechenault, S. Moulinet, M. Schillaci, and D. Vella, Inverse leidenfrost effect: Levitating drops on liquid nitrogen, *Langmuir* **32**, 4179 (2016).
 - [16] P. Chantelot and D. Lohse, Drop impact on superheated surfaces: Short-time dynamics and transition to contact, *J. Fluid Mech.* **928**, A36 (2021).
 - [17] P. Chantelot and D. Lohse, Leidenfrost effect as a directed percolation phase transition, *Phys. Rev. Lett.* **127**, 124502 (2021).
 - [18] J. Miguet, B. Scheid, L. Maquet, B. Darbois Texier, and S. Dorbolo, Thermal antibubbles: When thermalization of encapsulated leidenfrost drops matters, *Phys. Rev. Lett.* **131**, 184001 (2023).
 - [19] H. Kim, B. Truong, J. Buongiorno, and L.-W. Hu, On the effect of surface roughness height, wettability, and nanoporosity on leidenfrost phenomena, *Appl. Phys. Lett.* **98**, 083121 (2011).
 - [20] M. Jiang, Y. Wang, F. Liu, H. Du, Y. Li, H. Zhang, S. To, S. Wang, C. Pan, J. Yu *et al.*, Inhibiting the leidenfrost effect above 1000 °C for sustained thermal cooling, *Nature (London)* **601**, 568 (2022).
 - [21] P. Bourrienne, C. Lv, and D. Quéré, The cold leidenfrost regime, *Sci. Adv.* **5**, eaaw0304 (2019).
 - [22] L. Maquet, B. Sobac, B. Darbois-Texier, A. Duchesne, M. Brandenbourger, A. Rednikov, P. Colinet, and S. Dorbolo, Leidenfrost drops on a heated liquid pool, *Phys. Rev. Fluids* **1**, 053902 (2016).

- [23] B. Sobac, L. Maquet, A. Duchesne, H. Machrafi, A. Rednikov, P. Dauby, P. Colinet, and S. Dorbolo, Self-induced flows enhance the levitation of leidenfrost drops on liquid baths, *Phys. Rev. Fluids* **5**, 062701(R) (2020).
- [24] D. Mohaddes, P. Boettcher, and M. Ihme, Hot surface ignition of a wall-impinging fuel spray: Modeling and analysis using large-eddy simulation, *Combust. Flame* **228**, 443 (2021).
- [25] Z. Zhao, X. Huang, H. Sheng, Z. Chen, and H. Liu, Promoted stable combustion of alcohol-based fuel accompanied by inhibition of leidenfrost effect in a wide temperature range, *Energy* **234**, 121248 (2021).
- [26] D. Segawa, T. Kadota, S. Nakaya, K. Takemura, and T. Sasaki, A liquid film or droplet of miscible binary fuel burning on a heated surface at elevated pressures, *Proc. Combust. Inst.* **32**, 2187 (2009).
- [27] A. Chausalkar, C.-B. M. Kweon, and J. B. Michael, Multi-component fuel drop-wall interactions at high ambient pressures, *Fuel* **283**, 119071 (2021).
- [28] Z. Zhao, X. Huang, H. Sheng, and H. Liu, On promoted combustion stability of kerosene/ethanol blends at wide low temperatures: Fuel reactivity improvement and leidenfrost effect suppression, *Fuel* **315**, 123221 (2022).
- [29] P. Fu, L. Hou, Z. Ren, Z. Zhang, X. Mao, and Y. Yu, A droplet/wall impact model and simulation of a bipropellant rocket engine, *Aerosp. Sci. Technol.* **88**, 32 (2019).
- [30] X. Fan, F. Lin, S. Dorbolo, W. Wang, and J. Zou, Tunable self-extinguishing of dripping fire mediated by impacted substrates, *Int. J. Heat Mass Transf.* **223**, 125262 (2024).
- [31] S. Hidalgo-Caballero, Y. Escobar-Ortega, and F. Pacheco-Vásquez, Leidenfrost phenomenon on conical surfaces, *Phys. Rev. Fluids* **1**, 051902(R) (2016).
- [32] B. Sobac, A. Rednikov, S. Dorbolo, and P. Colinet, Leidenfrost effect: Accurate drop shape modeling and refined scaling laws, *Phys. Rev. E* **90**, 053011 (2014).
- [33] K. J. Baumeister, T. D. Hamill, and G. J. Schoessow, A generalized correlation of vaporization times of drops in film boiling on a flat plate, NASA TM X-52177 (1966).
- [34] E. W. Lemmon, M. O. McLinden, D. G. Friend, P. J. Linstrom, and W. J. Mallard, *NIST Chemistry WebBook* NIST Standard Reference Database Number 69 (NIST, Gaithersburg, MD, 2011).
- [35] G. Liu, L. Ma, and J. Liu, *A Handbook of Chemistry and Chemical Property Data* (Chemical Industry Press, Beijing, 2002).
- [36] See Supplemental Material at <http://link.aps.org/supplemental/10.1103/PhysRevFluids.10.043601> for Movie S1 presents five videos of inflamed ethanol drops with an initial volume of $V_0 = 240 \mu\text{L}$. The wall temperatures during recording are shown at the bottom of each video, demonstrating various evaporation modes of the inflamed drops. Movie S2 contains four videos that showcase the evaporation processes of both noninflamed and inflamed ethanol Leidenfrost drops. The drops have initial radii of $R_0 = 1.33 \text{ mm}$ (small drops) and 3.42 mm (large drops), with the wall temperature set at 200°C in each video.
- [37] A. L. Biance, C. Clanet, and D. Quéré, Leidenfrost drops, *Phys. Fluids* **15**, 1632 (2003).
- [38] K. J. Baumeister and T. D. Hamill, Creeping flow solution of the leidenfrost phenomenon, NASA TN D-3133 (1965).
- [39] K. Zhang, W. Gao, Y. Li, Z. Zhang, S. Shang, C. Zhang, X. Chen, and K. Sun, Lower flammability limits of ethanol, acetone and ethyl acetate vapor mixtures in air, *J. Loss Prev. Process Ind.* **74**, 104676 (2022).
- [40] X. Ma, J.-J. Liétor-Santos, and J. C. Burton, Star-shaped oscillations of leidenfrost drops, *Phys. Rev. Fluids* **2**, 031602(R) (2017).
- [41] D. Pietschmann, R. Stannarius, C. Wagner, and T. John, Faraday waves under time-reversed excitation, *Phys. Rev. Lett.* **110**, 094503 (2013).
- [42] V. Babrauskas, Estimating large pool fire burning rates, *Fire Technol.* **19**, 251 (1983).
- [43] S. Parag and V. Raghavan, Experimental investigation of burning rates of pure ethanol and ethanol blended fuels, *Combust. Flame* **156**, 997 (2009).
- [44] X. Fan, Dataset for inflamed Leidenfrost drops <https://doi.org/10.6084/m9.figshare.28597205.v1> (2025).